Anomalous spin exciton with a magnetoroton minimum in a quantum Hall ferromagnet at a filling factor $\nu = 2$

A. B. Van'kov and I. V. Kukushkin

Institute of Solid State Physics, RAS, Chernogolovka 142432, Russia
and National Research University Higher School of Economics, Laboratory for Condensed Matter Physics, Moscow 101000, Russia

In ZnO-based two-dimensional electron systems with strong Coulomb interaction, the anomalous spin-exciton branch is revealed. As probed by inelastic light scattering, in a ferromagnetic quantum-Hall state with the filling factor $\nu = 2$, a spin exciton has a negative momentum dispersion with steepness dependent on the electron density. The negative dispersion of the spin exciton is associated with its interaction with higher-energy spin-flip modes that exist near $\nu = 2$. Surprisingly, the anti-Stokes light scattering on spin excitons at ferromagnetic state $\nu = 2$ is amplified by orders of magnitude, indicating the macroscopic accumulation of these excitations. The experimental findings are confirmed by the exact diagonalization method—these calculations show a magnetoroton minimum in the dispersion of spin excitons and also the attractive interaction between magnetoroton spin excitations.

I. INTRODUCTION

The physics of collective effects in two-dimensional electron systems (2DESs) has brought about a new stream of puzzles with recent progress in the fabrication of new ultrapure heterostructures with strong interaction—ZnO, AlAs, GaN, SiGe, and others. Among them, the material parameters of MgZnO/ZnO heterostructures enable the most direct access to the properties of strongly interacting electrons, since the material is single valley, with weak spin-orbit interaction and, most importantly, hosts 2D electrons with high values of Wigner-Seitz parameter $r_s \gg 1$ at extra-high mobilities [1]. The quality of ZnO-based systems has recently reached a level sufficient for the brightest collective phenomena—fractional quantum Hall effect (QHE) [2], Stoner transition with and without quantizing magnetic field [3,4], and even Wigner-crystallization [4] at $r_s \sim 30$.

The explored collective effects in strongly interacting 2DESs raise many questions concerning the modification of their energy spectrum, the microscopic structure of the ground state, and the properties of excitations. The increased role of many-particle interaction, dominating over the kinetic energy, modifies the character of electron-electron correlations and complicates their analysis due to the lack of a small parameter in theory. It is thus expedient to investigate the properties of the simplest excitations in 2DESs, which determine the stability of many-particle phases and their energy spectrum. The easiest way to do this is in the QHE regime: the system is incompressible, the kinetic energy of electron states is completely quantized, and the electron energy scales in the magnetic field can be separated.

In QHE states, the collective excitations, called magnetoexcitons [5], often present quasiparticles with intriguing properties. Magnetoexcitons carry information of the many-particle properties of QHE systems, their energy scales, define the energy gaps of incompressible states [6,7]. In specific cases, the lowest energy magnetoexcitons acquire extraordinary properties, such as extra-long lifetimes in the millisecond/second scale [8], magnetoroton [9], and magnetogravitonlike [10] peculiarities in dispersions, bose, or anyon statistics. Physics becomes more and more fascinating when these quasiparticles accumulate macroscopically [11,12] in the system and even form coherent condensates.

For direct-gap semiconductor heterostructures, such as MgZnO/ZnO, the energy and dispersion of collective excitations can be effectively probed by inelastic light scattering (ILS or Raman method). In different states of the QHE, the set of excitations is specific, and the many-particle contributions to their energies correspond to exchange and correlation properties. Nontrivial findings have been explored at $r_s \gg 1$ in the state of quantum Hall ferromagnet at $\nu = 1$. The most notable change concerns the scale of exchange interaction of spin-polarized electrons [13,14]—it is suppressed dramatically from the level $e^2/\epsilon l_B$ to values of the order of cyclotron energy $\hbar\omega_c$.

At other integer filling factors, electron-electron correlations can rearrange the Landau level (LL) sequence, which results in phase transitions. In particular, at $\nu = 2$ the system switches from a paramagnetic (PM) to ferromagnetic (FM) spin configuration [2,3,15]. This QH state provides the most straightforward platform for the controllable FM transition—the energy competition between two spin-configurations, where crucial parameters, such as Zeeman, cyclotron splittings, and exchange energy, are all separately controllable. Meanwhile, the instability mechanism at $\nu = 2$ has just been explicitly described for one direction—from a PM to FM state [16]. There, the energy gap is determined by the lowest spin component of cyclotron spin-flip magnetoexcitons

(CSFMs)—thoroughly studied in GaAs structures [17,18] and ZnO-based systems [16]. These excitations are shifted fairly below the cyclotron gap due to the correlation energy; moreover, they demonstrate a magnetoroton minimum at $q\ell_B \sim 1$. CSFM excitations in magnetoroton minimum are extremely long-lived; they can accumulate and form macro-occupied coherent states [11]. Eventually, the attractive interaction between them leads to the dramatic gain in energy, their softening, and avalanchelike spin-flip process in the system—FM instability.

The description of reverse transition requires analysis of excited states for the FM phase, which is complicated due to the strong Landau-level mixing and problems even for a description of the FM ground state. The conventional Hartree-Fock approximation (HFA) fails to describe the transition in terms of soft spin-flip excited states—all excited states seem to have energies above Zeeman splitting [19]. So, the microscopic mechanism of the Stoner transition at $\nu = 2$ and the energy spectrum of the FM phase remained obscure.

Here we address this problem in a complex manner by combining the Raman scattering method for probing the lowest-energy magnetoexcitons and the exact diagonalization method for calculating the energy spectrum of the system. Raman scattering studies of the series of high-quality MgZnO/ZnO heterostructures enabled us to reveal anomalous momentum-dispersion of the lowest in energy spin excitons (SEs) in the FM phase $\nu = 2$. In contrast to magnons in conventional ferromagnets or well-known quantum Hall ferromagnet at $\nu = 1$, here the excitation has a negative momentum dispersion with steepness strongly dependent on the electron density. The theoretical description of spin excitations was carried out by the exact diagonalization of the electron spectrum and, alternatively, in terms of a single-mode approximation for a system of Fermi-liquid quasiparticles at their Landau levels. Both approaches give a comparable answer and agree with the experiment. The anomalous dispersion of the lowest SE is the result of its hybridization with higher spin-flip modes. Unexpectedly, the deep magnetoroton minimum appears below Zeeman energy in the dispersion of the SE. Another impressive fact is that we found experimental evidence of the macroscopic accumulation of these low-energy SEs as a nonlinear growth of the anti-Stokes Raman signal. It indicates the formation of a macroscopic ensemble of SEs. The prerequisites for accumulation of SEs also follow from their calculated dispersion with a magnetoroton minimum, high density of states, and attractive interaction.

II. EXPERIMENTAL TECHNIQUE

Experimental studies were performed on five MgZnO/ZnO heterostructures grown by molecular beam epitaxy [1]. A 2DES was formed in the ZnO layer near the heterointerface, occupying one size-quantized subband. Electron densities in samples ranged from $1.75\times$ to 4.5×10^{11} cm^{-2} and low-temperature mobilities exceeded 400 000 cm^2/V s. The measurements were carried out in a ^{3}He vapor evacuation cryostat with a bath temperature $T= 0.35$ K in magnetic fields up to 15 T. To achieve the conditions of FM instability at a filling factor $\nu = 2$, it was required to have an oblique orientation of the magnetic field to the normal of the sample.

In this case, the ratio between the values of the Zeeman and cyclotron energies changed. For each of the samples, this orientation of the magnetic field was chosen based on the known phase diagram of the FM transition in the coordinates of the electron density versus the tilt angle [3]. For the investigated heterostructures, the slope ranged from 12° to 42°. Optical experiments were performed using a tunable Ti-Sp laser doubled in frequency with a wavelength in the range 366–367 nm near the direct optical ZnO gap. The magnetic field evolution of the photoluminescence signal from 2D electrons was studied to determine Landau quantization conditions, corresponding to integer filling factors, and to track the signatures of the FM phases or PM phases in the QHE state with $\nu = 2$. The inaccuracy in determining the magnetic field corresponding to a phase transition point at $\nu = 2$ was below $\delta B \sim 0.05$ T. The dispersion of collective excitations was measured by the method of resonant ILS with a tunable transferred momentum. For photoexcitation of the electronic system and recording the scattered light signal, two quartz multimode optical fibers were used, oriented at different angles to the sample surface. The tilt angles of the magnetic field and quartz fibers were controlled separately, using the rotational stage shown in Fig. 1(a). The transferred momentum was set by the difference between the projections of the incident and scattered photons on the 2DES plane and reached values in the range $0.4\times$ to 3.0×10^5 cm^{-1}. The lower boundary of this range was associated with the influence of stray laser light. The upper limit of the range was limited by trigonometry at close to the tangent orientation of the fibers to the surface. The optical fibers' numerical aperture was NA=0.11, which led to an easily calculated uncertainty of the transferred momentum. To achieve maximum accuracy in measuring the energy of collective excitations, we used a spectrometer in combination with a CCD camera providing a spectral resolution of 0.03 meV, with further refinement of the position of the peaks by the method of statistical averaging with $N \sim 20 - 30$ of raw spectra taken into account. The total error in determining the position of the peaks reached 3-4 μeV.

III. MEASUREMENT OF SPIN EXCITON DISPERSION

The SE is the simplest magnetoexciton for FM QHE states. Thank to Larmor's theorem, its energy at small momenta is *a priori* known—it is equal to the single-particle Zeeman splitting. It is also a long-living excitation, so its natural linewidth lies in the GHz range and looks extremely fine in optical spectra. Thus, Raman peak at energies close to E_z in FM states can be easily identified as SE. The tricky thing is to discern a subtle momentum dispersion for the parameters in ZnO. In the case of the FM state $\nu = 1$, the long-wavelength variance of SE energies was on the level of tens of microelectronvolts [14]. So, the seemingly cognate case of $\nu = 2$ ferromagnet requires no less accurate measurements. As shown in Ref. [14], the statistical processing of an array of similar Raman spectra makes it possible to surpass the peak position accuracy beyond the spectrometer resolution. Analogously in the actual study, we analyzed ensembles of SE Raman spectra, taken at different laser wavelengths, to determine Raman shifts most accurately. Then we studied the momentum dispersion of excitations while changing the transferred momentum. An idea
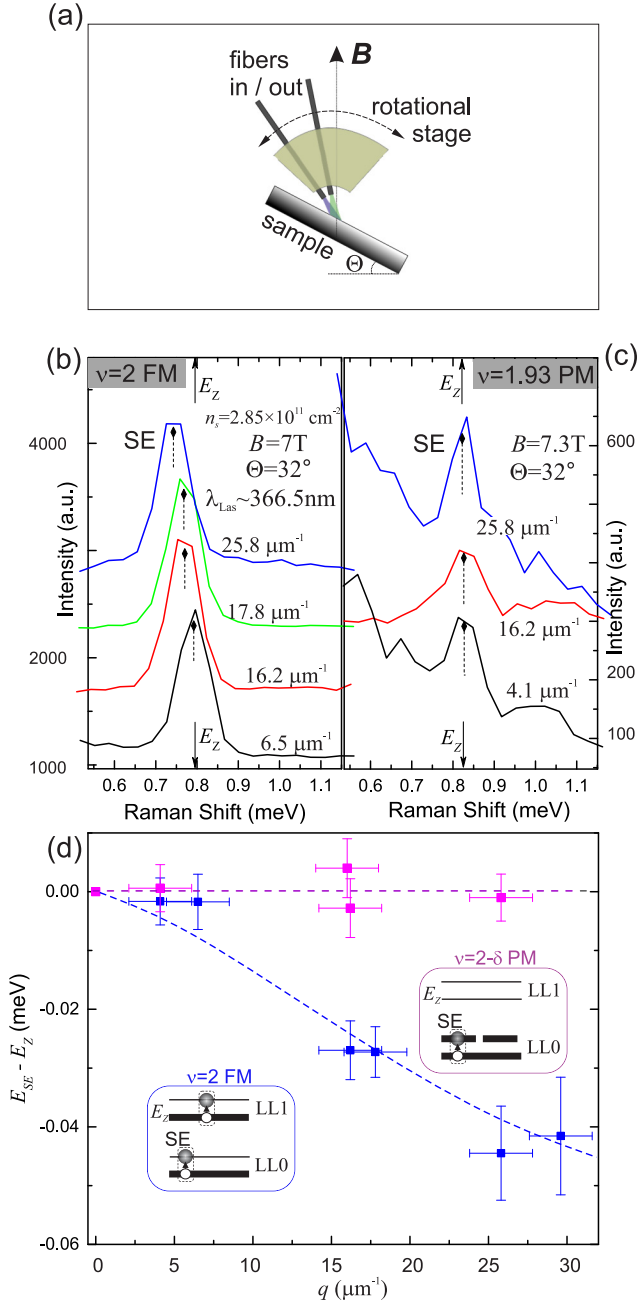
FIG. 1. (a) The schematic picture of the rotational stage, used for the Raman experiment with variable transferred momentum and in tilted magnetic field. (b) The cascade of Raman spectra of spin exciton at ferromagnetic $\nu = 2$ and different values of the in-plane momentum (indicated next to curves). The flags are set on the centers of mass of the peaks. The calculated Zeeman energy position is shown by arrows. (c) The same sequence but for the paramagnetic state with $\nu = 1.93$. Here the SE dispersion is negligible. (d) The processed momentum dispersion of SEs from panels (b) and (c). The single-particle Zeeman terms are subtracted from the energies. The dashed lines serve as a guide for the eyes. The inset shows a single-particle representation of SEs for FM and PM phases.

of the SE dispersion magnitude can be obtained from the set of spectral data shown in Fig. 1(b) for the sample with $n_s = 2.85 \times 10^{11}$ cm^{-2} at FM phase $\nu = 2$. Contrary to the

case of a quantum Hall ferromagnet with $\nu = 1$, the energy at FM phase $\nu = 2$ decreases with momentum.

Undoubtedly, the behavior of SE is determined by the spin configuration of the ground state and the corresponding exchange contributions. It can be explicitly seen by controlling the magnetic field parameter and entering the PM phase $\nu = 2$ to explore an abrupt modification of SE energy. Measurements at strict PM $\nu = 2$ are impossible, but a deviation to $\nu = 2 - \delta$ to introduce a subtle asymmetry in occupation of spin sublevels enables to measure a PM SE. It reappears in the Raman spectra, although with a significantly smaller scattering cross section [Fig. 1(c)]. The SE-dispersion data at FM and PM phases are plotted in Fig. 1(d): in the range of accessible momenta, FM SE has a pronounced negative dispersion, whereas the PM SE is practically dispersionless in the same range of wave vectors. So, the compensation of exchange energy contributions in the spin-symmetric PM phase near $\nu = 2$ completely cancels the many-particle contribution to the SE energy. The flattening of the dispersion follows even from a simple consideration in the HFA model [5] and can be given straightforwardly: $E_{SE}^{2-\delta}(k) = E_Z + \delta J(ql_B)^2$. Therefore, for filling factors $\nu = 2 - \delta$, we obtain just the bare value of a Zeeman energy.

The FM phase of $\nu = 2$ is qualitatively different since half the electrons have inverted spin projections and the exchange contributions are pronounced. Unlike magnons in conventional ferromagnets or those in quantum Hall ferromagnets at $\nu = 1$, the dispersion of our SE is negative and is not described by a quadratic law. Consequently, the parameter of spin stiffness is devoid of strict sense. Nevertheless, studies on several samples with different electron densities show that the dispersion steepness grows substantially with electron density (see Fig. 2). Not all the data sets imply straight line approximations, and the eye-guide lines were drawn in a splinelike manner. It will be shown below that dispersions of SEs at $\nu = 2$ are indeed of complicated functional form and, as a rule, contain inflection points. The detailed knowledge of these features was not pursued in the current experiment. A much more important finding is that SE dispersion is negative everywhere—even for the lowest density 2D system $n_s = 1.75 \times 10^{11}$ cm^{-2}, where FM transition occurs naturally, already at normal B orientation.

IV. INTERACTING SPIN EXCITONS AT FERROMAGNETIC STATE $\nu = 2$

Below we consider the two approaches to the problem of spin excitations at $\nu = 2$—the exact diagonalization of the energy spectrum for a finite number of electrons at few lowest Landau levels and a statically screened HFA. First, we will show numerically that the observed negative slope of the SE dispersion at $\nu = 2$FM at small momenta is a prerequisite of a magnetoroton minimum. Then, using the screened HFA, the negative dispersion of SEs will be explained in terms of the four hybridized lowest spin-flip modes, involving states at zeroth, first, and second LLs.

To describe such excitations, above all, it is necessary to start from the ground state with full spin polarization, which was experimentally confirmed in Refs. [2,3,16] and described as a FM arrangement of electrons on a few lowest LLs. Due
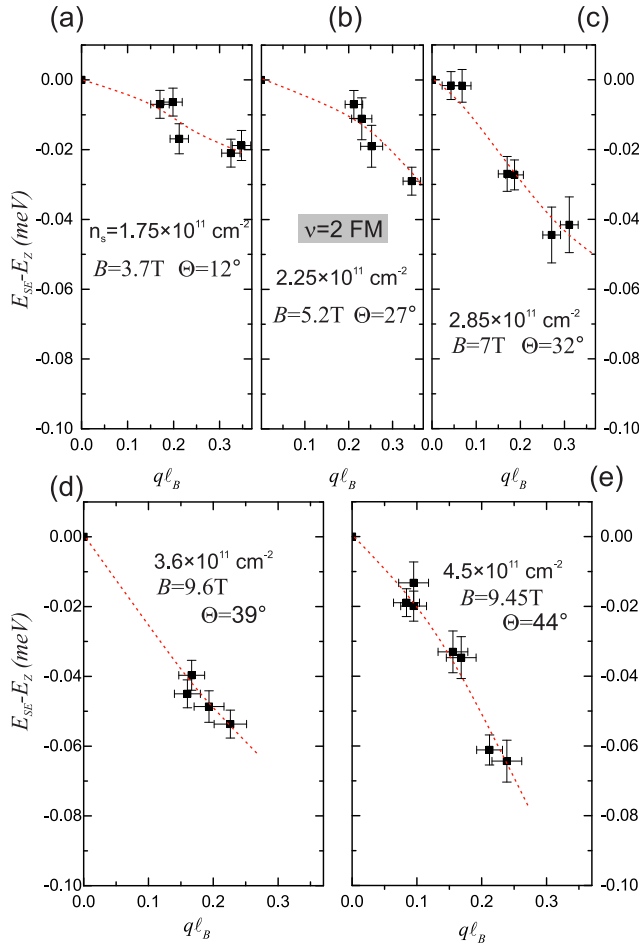
FIG. 2. Plots of SE dispersions at the ferromagnetic phase of $\nu = 2$ in the five studied samples. The energies are given minus the Zeeman term. The magnetic fields and tilt angles are indicated on the graphs. The abscissa is given in dimensionless wave vector $q l_B$ for corresponding normal magnetic fields. The lines are guides for the eyes.

to the essential LL-mixing effect for the parameters of considered 2DESs ($r_s > 5.5$), the ground state has an essentially correlated structure and should be calculated numerically. In the present paper, it was sufficient to consider interacting electrons in the basis of states on three lowest Landau levels. The exact diagonalization procedure was performed separately for the FM ground state and several excited states with different total spin values. The discreteness of the numerical problem was restricted by the number of flux quanta (or LL capacity) N_S from 9 to 10 and the twice larger number of electrons at $\nu = 2$ in the rectangular torus geometry, subject to periodical boundary conditions [20]. So, the momenta of the neutral excited states in the magnetic Brillouin zone are of the order $q l_B \sim \sqrt{2\pi/N_S}$. The Coulomb matrix elements used for the calculations are taken from Ref. [21]. The influence of the higher unaccounted LLs was also introduced to the numerical procedure via the screening factor $\epsilon_s(q)$ in the Coulomb potential (see below). The single-particle 2DES parameters, essential for calculations, were taken from other experimental studies [22,23] and were the following: Lande factor $g^*=1.95$,

cyclotron mass $m_c = 0.3 m_0$, dielectric constant is $\varepsilon_{ZnO} = 8.5$. We also took into account the influence of the finite thickness of 2DES in the growth direction, introducing the geometric form-factor $F(q)$ to the Coulomb potential.

Since the calculated ground and excited states of $\nu = 2$ FM are impossible to illustrate and analyze, we better try to simplify their structure to the comprehensible sketch with filled and empty LLs with electron transitions between them. In this representation, there exist just four single-mode and simplest spin-flip transitions [shown in diagrams I–IV of Fig. 3(a)]. However, there are also a huge number of composite multiexciton transitions, like diagrams V, VI, etc. For the actual parameters of the experimental samples, the LL-mixing parameter at $\nu = 2$ exceeded the value 5.5. Therefore, it is natural to assume that the variety of multiexciton components in the structure of both the ground and excited states is enormous. Despite this complexity, the resulting solution of the problem for sure contains at least one spin-flip mode, the energy of which is strictly equal to the Zeeman gap at $q = 0$, according to Larmors theorem [24]. We will call it, of course, the SE or sometimes SE1, since, as will be shown below, the mode is not independent and mixes strongly with others closest in energy spin-flip modes.

Exact diagonalization calculations intrinsically take into account all the electron correlations within three lowest LLs, and the eigen spin-flip modes involve all mixed transitions. The calculated SE dispersion for the sample with $n_s = 2.85 \times 10^{11}$ cm^{-2} is shown by open symbols in Fig. 3(b) along with experimental points in the range of wave vectors from 0 to $q l_B = 1.7$. Despite the rough discreteness of the calculated data associated with the small capacity of LLs $N_s = 9$ and 10, it is clear that the slopes of the calculated data are in good agreement with the experimental trend. In addition, the calculations do show a noticeable magnetoroton minimum in the range of momenta roughly $q l_B \sim 0.5 - 1.0$. The parameters of calculated dispersions depend on the electron density. However, we do not see much sense in analyzing the functional laws of the long-wavelength parts due to the insufficient smoothness of data sampling. Instead, we will switch to the alternative theoretical approach and try to interpret the negative dispersions qualitatively in terms of the HFA.

It should be noted right away that the FM phase of $\nu = 2$ is not necessarily the result of exchange-driven Stoner transition. As established earlier in a series of magnetotransport studies of 2DESs in semiconductor heterostructures with much weaker interaction [25–29], the phase transition takes place for Ising ferromagnets in tilted magnetic fields. The primary condition is that Zeeman splitting represents a multiple of the cyclotron energy. In the case of small r_s values, the energy spectrum of Ising ferromagnets can be duly described in terms of perturbation theory and hence HFA [5] is applicable for the collective excitations. The idea of the following consideration is to develop an analytic procedure for calculation of SEs in the $\nu = 2$ FM state and then to smoothly extrapolate the results to the case $r_s \gg 1$, with the difference that electron LLs are transformed to some effective LLs for Fermi-liquid quasiparticles, which interact via screened Coulomb potential [30]. This approach is nothing but qualitative description, but it has proved to be appropriate in recent studies of strongly interacting QHE systems [13,16,21]. However, the explicit
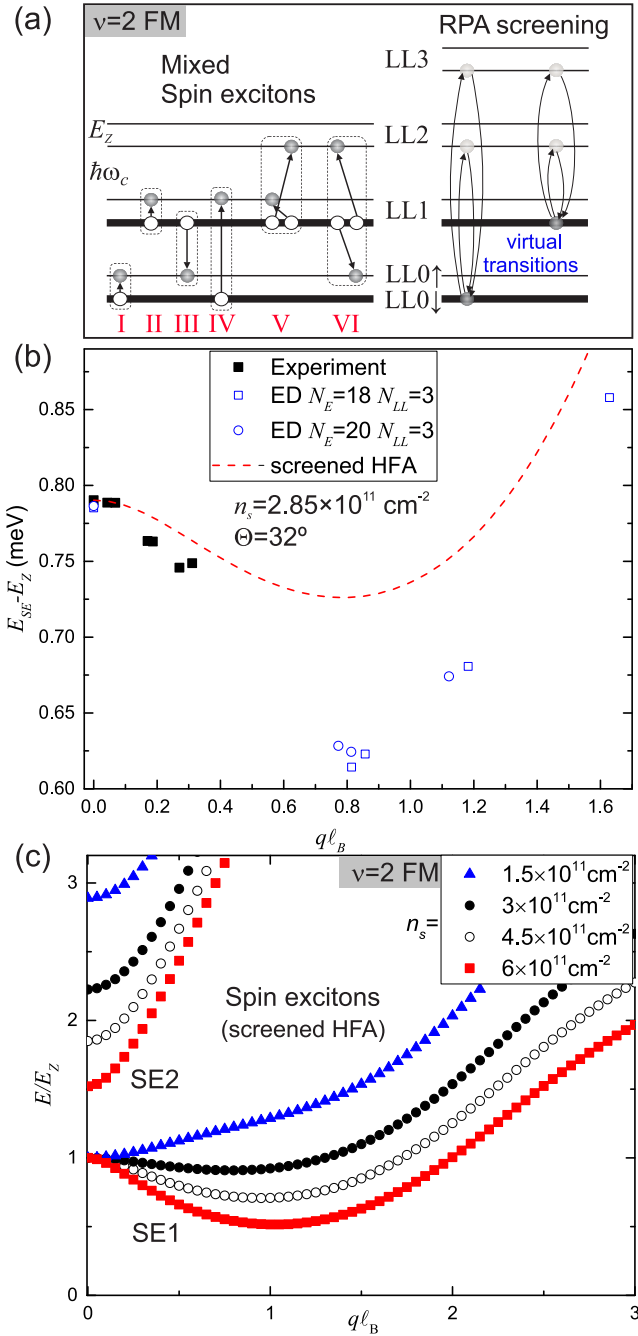
FIG. 3. (a) Left: The single-particle representation of the simplest spin-flip transitions at the ferromagnetic phase at $\nu = 2$. Filled spin Landau levels are drawn by bold lines. Single-mode transitions (I–IV) are explicitly accounted in the HFA calculations below. Double-mode states V and VI with the same set of quantum numbers are examples of unaccounted terms. Right: The illustration of screening processes, caused by virtual inter-LL transitions, contributing to the RPA (random phase approximation) static dielectric function $\varepsilon_s(q)$ (see the text). (b) The comparison of SE momentum-dispersion at $\nu = 2$ FM for the sample with $n_s = 2.85 \times 10^{11}$ cm^{-2} obtained in experiment (solid symbols), exact diagonalization (open symbols) and screened HFA. (c) Dispersion curves of the two lowest SEs at $\nu = 2$ FM for four different electron densities.

Landau quantization for Fermi-liquid quasiparticles at $r_s \gg 1$ was indeed seen by magnetophotoluminescence [31,32].

The weakening of Coulomb interaction of quasiparticles occurs due to the polarizability of 2DES caused by virtual transitions between LLs. The 2D-Fourier component of the Coulomb potential in this approach is divided by a static dielectric function: $V(q) = \frac{2\pi e^2}{\varepsilon q} \frac{1}{\varepsilon_s(q)}$. The latter can be calculated in the random phase approximation [21]:

$$\epsilon_s(q) = 1 - \frac{2\pi e^2}{\varepsilon q} \chi_{nn}^0(q, \omega \to 0^+).$$

Here, $\chi_{nn}^0(q, \omega)$ is the retarded density response function, which takes the following form for a noninteracting 2DES in a magnetic field:

$$\chi_{nn}^0(q) = \frac{1}{2\pi l_B^2} \sum_{\sigma} \sum_{k,m} |F_{k,m}(q)|^2 \frac{\nu_{m,\sigma} - \nu_{k,\sigma}}{(m-k)\hbar\omega_c}, \quad (1)$$

where $\nu_{m,\sigma}$ is the filling factor of a LL m with a spin index σ. The estimates of $\epsilon_s(q)$ can be made for the unperturbed filling factors $\nu_{m,\sigma}$. If one introduces this suppressive factor to the Coulomb interaction of charged quasiparticles, the effective r_s values get strongly reduced and the application of the single-mode approximation becomes justified. For the FM ground state $\nu = 2$, the basis of four simplest spin-flip transitions has been treated to find eigenvalues and eigenvectors of resulting spin-flip modes.

Here, at $\nu = 2$ FM, the ground state of the system is equally represented by two kinds of quasiparticles—with different orbital quantum numbers LL0 and LL1 and the same spin projection. Therefore, essential mixing will occur between the set of spin-flip transitions within the two lowest LLs, as depicted by diagrams I–IV in Fig. 3(a). The many-particle energy terms and corresponding matrix elements have been calculated in the spirit of well-known HFA [5,19], giving the first-order energy corrections at small effective r_s values. The four magnetoexcitons can be given in notation of excitonic operators,

$$(I) = Q_{0\bar{0}}^+, (II) = Q_{1\bar{1}}^+, (III) = Q_{1\bar{0}}^+, (IV) = Q_{0\bar{1}}^+, \quad (2)$$

with matrix elements given in Ref. [19].

The diagonalization of this 4×4 matrix results in the four eigenmodes. The lowest one definitely has the Zeeman energy at $q\ell_B = 0$. HFA calculations for this SE1 mode are compared with experimental data and the exact diagonalization results [Fig. 3(b)]. The magnetoroton minimum in HFA calculations is roughly three times more shallow. The numerical discrepancy is rather expected since too many issues are undetermined in the HFA consideration. First, it is the adequacy of the screening function $\varepsilon_s(q)$, dramatically influencing the answer, but also significant are the omitted multiexcitonic contributions within the lowest two LLs. Nevertheless, the origin of anomalous negative dispersion of SE1 gets evident from this qualitative result—it is the result of a dramatic repulsion between two modes, SE1 and SE2. To illustrate this, the calculated dispersions are shown in Fig. 3(c) for

four different electron densities. The energy scale for each electron density has been normalized to its Zeeman energy E_Z at $\nu = 2$ to explore the relative depth of the magnetoroton minimum.

The advantage of this simplified single-mode representation is that we can identify the two interacting modes—their structure can be obtained as an eigenvector in the excitonic basis (I)–(IV). At $q\ell_B = 0$, SE1 is just a cophase combination of the simplest spin transitions (I) and (II), and SE2 is a pure transition (III). Exciton-mixing terms emerge at nonzero momenta, the modes SE1 and SE2 couple and in the vicinity of magnetoroton minimum the SE1 mode is already a linear combination of three transitions (I)–(III) with the third component dominating. In the short-wave limit, SE1 is entirely represented by (III). The calculated composition of the modes depends on momentum and electron density. It is also noteworthy that higher transitions, such as (IV), influence the structure of low-energy SE1 in a minor way—its fraction never exceeds $\sim 4\%$.

It can be seen that the steepness of the negative fragment of the SE1 dispersion strongly depends on the proximity of mode SE2 [the corresponding symbols in Fig. 3(c) are given in pairs], and is associated with the mutual repulsion of the two modes. The repulsion becomes stronger as the energies are closer at $q = 0$. For the case of proximity at $q = 0$, the initial slope of dispersion is nearly linear (red symbols) with a deep magnetoroton minimum, but for the case of the smallest shown electron density (blue symbols), the SE1 dispersion increases monotonically. The disappearance of the calculated magnetoroton minimum occurs in the range $1.5–2 \times 10^{11} cm^{-2}$, close to the critical density $n_s = 1.8 \times 10^{11} cm^{-2}$ for spontaneous FM transition at $\nu = 2$, found experimentally for ZnO [2,16]. This finding suggests that the existence of the magnetoroton minimum in SE1 dispersion is crucial for the possibility of the phase transition FM-PM at $\nu = 2$ as well as the roton minimum in CSFM excitation of a PM phase is needed for the reverse transition [16]. The tilting of the magnetic field causes just change in a Zeeman contribution to the energies of spin excitations. Therefore, it stabilizes the FM phase and destroys the PM phase.

Although the experimental data for SE1-mode in this study are extensive, its counterpart SE2 has still been behind the scenes. The problem seems to be in the vanishingly small Raman cross-section for the SE2 at $\nu = 2$ FM state. This mode may have some symmetry restrictions for Raman polarizability because of an anti-phase combination of spin-flip transitions. To overcome this and to confirm the existence of SE2, we induced an anticrossing between these two modes by varying the filling factor parameter. Both lines should become visible when they are brought to anticrossing. In Fig. 4, the energies of the two lowest excitations are plotted as a function of the magnetic field for one of the samples. The experimental parameters are indicated on the plot. The tilt angle is chosen above the critical value of the FM transition to have a stable FM phase in some vicinity of $\nu = 2$. From the plot, one can see that SE1 is the only excitation visible around $\nu = 2$. While the other higher energy excitation is descending abruptly from above on both sides of $\nu = 2$ at $\Delta B \sim 0.5$ T. Their evident anticrossing proves the spin-nature of the second mode, which is highly likely SE2.
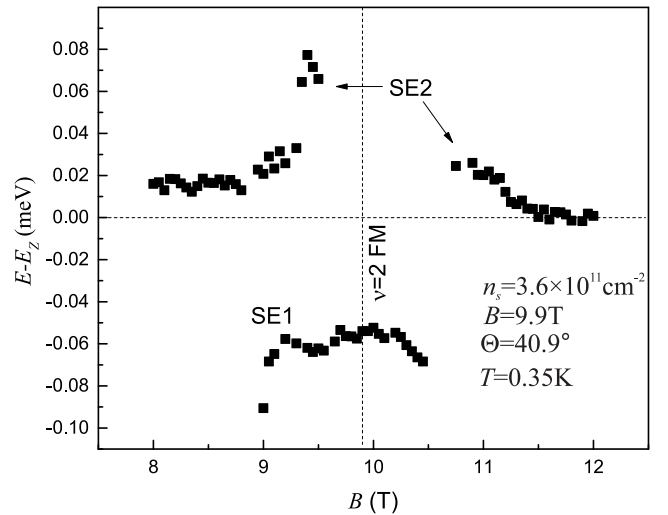

FIG. 4. The plot of measured energies of the two interacting modes SE1 and SE2, probed by Raman scattering nearby ferromagnetic state at $\nu = 2$. Note the increased magnetic field tilt angle $\Theta = 41°$ provides stable FM phase not just at $\nu = 2$, but also in vicinity.

V. CLUMPING OF SPIN-EXCITONS

The presence of magnetoroton minima for the lowest-energy spin-flip excitations in both phases of $\nu = 2$ is a prerequisite for the FM transition. However, in both cases the depths of these roton minima in the transition point are quite insufficient for the single spin-flip transition to soften completely. As was shown in the case of the PM phase, the softening first occurs for multi-CSFM complexes, which gain in energy. Here in this paper we need to further elaborate properties of magnetoroton SE1 modes to accomplish the mechanism of the reverse phase transition. We only have to prove that these excitations attract and tend to clump in complexes. For this the exact diagonalization was performed for the states with change in total spin $\Delta S_z = +2$, i.e., double spin-flip processes. Fig. 5 displays the result of calculation for the electron density $n_s = 3.6 \times 10^{11} cm^{-2}$ and the tilt angle $\Theta = 39°$. The plot contains dispersion-data for the two lowest modes SE1, SE2, and for the double spin-flip transition (red asterisks). Most interesting is the double spin-flip energy in the point $q\ell_B = 0$ – its energy is significantly less not only than double Zeeman energy, but also than the double energy of magnetorotons, as indicated by a parallelogram scheme. It is strong evidence that there exist processes consisting of two clumped (or twin) SEs, which are energetically more favorable than two separate SE1s. These double-mode excited states can be generally described as a convolution of the two SE-modes:

$$|\text{twin} - SE(\vec{k}) >= \int f(q)|SE1(\vec{k}+\vec{q}) > |SE1(-\vec{q}) > d^2q.$$

The most favorable calculated state is that with $\vec{k} = 0$, that is clumping of the two modes with opposite momenta. It is clear, that the largest contribution to the sum will emanate from SE1 components with the highest density of states, i.e., in the magnetoroton minimum. Therefore, the twin-SE mode
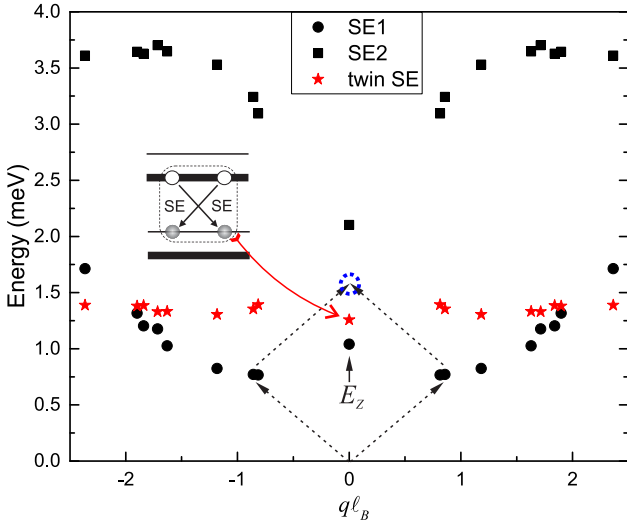
FIG. 5. Calculated dispersion laws for the two lowest hybrid modes SE1 and SE2 and the dispersion of the twin-SE mode in the FM phase $\nu = 2$. The diagram shows the double-exciton diagram of the twin-SE as the two clumped magnetoroton SEs with opposite momenta.

can be viewed as the two clumped magnetorotons (see Fig. 5). Finally, the energy gain for that excitation relative to the double magnetoroton energy proves that these SE1 modes interact attractively and can form stable multi-SE1 complexes causing phase instability.

VI. MACROSCOPIC ENSEMBLES OF SPIN EXCITONS

The integer spin of SE1, their high density of states in the magneto-roton minimum and attractive interaction open the opportunity to form macroscopic ensembles or even condensates. In the current experiment, we do not probe the lifetimes of SEs, but in a close analogy with their PM counterparts CSFMs at $\nu = 2$, the spin-flip excitations in the magnetoroton minimum may have extraordinarily long lifetimes, in the range of milliseconds [8] or even seconds [12]. In the previous sections, the experimental conditions for Raman scattering on SEs have been chosen simply for probing them. These conditions concerned both laser wavelength and its intensity. For resonant Raman scattering, the laser wavelength is chosen in the range of direct interband transitions for the 2D system, but the oscillator strength of these transitions and the resulting enhancement of a Raman process depend on the selection rules and the occupation of states in the conduction band. Working with a laser wavelength in the spectral range of PL transitions for resident 2D electrons has an advantage of stronger Raman enhancement but a disadvantage of multiple parasitic spectral lines of photoluminescence. These experimental conditions have been chosen here for more effective pumping of SEs at $\nu = 2$FM. The expected result of the resonant pumping is not just enhancement of spectral light, but possibly activating a nonlinear response of the system. It manifested in a very unexpected way—the anti-Stokes Raman peak of SE1 appeared in the spectrum. Figure 6(a) shows the spectrum of the sample with $n_s = 3.6 \times 10^{11}$ cm^{-2} at $\nu = 2$FM and the resonant laser
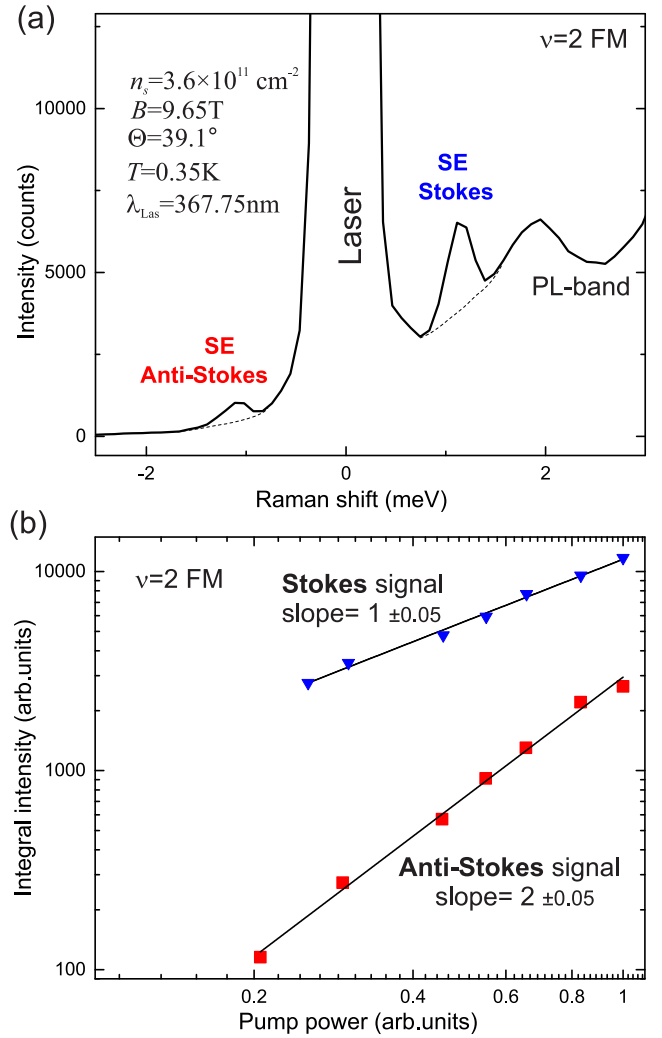

FIG. 6. (a) The resonant Raman spectrum of the lowest SE mode, showing an anomalously strong signal of anti-Stokes component. The experimental details are given in the graph. (b) The log-log power-intensity dependence of both the Stokes and anti-Stokes components of SE. The fitted slope values are signed next to the data plots.

excitation. The ratio of anti-Stokes and Stokes components is roughly 1:5, which is fascinating, since the thermodynamic ratio between them should be about $e^{-E_{SE1}/kT} \approx 10^{-15}$. This enormous anti-Stokes enhancement is definitely due to the accumulation of SE1s in the system and transferring it to an essentially nonequilibrium state. The macroscopic accumulation of SE1s in the system is also confirmed by studying the power dependence of Raman lines. In Fig. 6(b), the two plots show the growth laws of the Stokes (blue) and anti-Stokes (red) components. The log-log scale enables us to accurately establish the linear growth of the Stokes and quadratic growth of the anti-Stokes signal. Since scattered intensity always has a proportionality to the pump intensity, we conclude, that the quantity of SE1s participating in the Anti-Stokes scattering is also proportional to the pump intensity. So, they do accumulate in the system. It is important that the maximum pump

power used for this portion of experiment is not higher than that for probing SEs in previous sections. Unfortunately, we were unable to further increase the power to explore further nonlinear events for SE1s. The experiment at enhanced powers is a subject for future experiments.

VII. DISCUSSION

The formation of the quantum Hall ferromagnet at $\nu = 2$ and its thermodynamic properties have been experimentally studied previously in ZnO by magnetotransport and optical methods [2,33]. Some facts have been described in an empirical model of Ising ferromagnets with crossing spin-LLs. Nevertheless, the single-particle model of crossing LLs, perfectly applicable to other semiconductor systems, required a modification in the case of strongly interacting electrons in ZnO, namely, the orbital and spin splittings of LLs had to be renormalized due to Fermi-liquid effects. The energy spectrum gets essentially many-particle around a critical density $n_s = 1.8 \times 10^{11}$ cm^{-2}—there the tilting of the magnetic field is no longer required to trigger the FM transition; the FM phase is the only possibility for $\nu = 2$.

The current study sheds light on the microscopic mechanism of such many-particle transformations of the energy spectrum, which determines the stability of the phases. The experimental finding of the negative dispersion of the lowest energy SE was traced for the range of electron densities. The dispersion gets steeper at higher densities. Despite the limited accuracy of the used numerical simulations at $r_s \gg 1$, the same trend in SE dispersion has been confirmed numerically, suggesting that exact diagonalization is adequately applicable to the problem. It is a strong argument in favor of the calculated magnetoroton minimum.

The simplified approach to the spin-flip modes via statically screened HFA is far from being accurate, but it enabled unravelling the SE mode structure. According to this calculation, the main contribution to the formation of the roton minimum comes from the spin-flip component, returning electrons from LL1 back to LL0. This transition is exactly reverse to the lowest energy excitation of the PM phase CSFM. The close analogy of the properties of the lowest energy spin excitations in PM and FM phases suggests that mechanisms of the two phase transitions are also very similar—nucleation of multiexciton complexes softened in energy. It is not even so important how exactly the functional form of dispersion is arranged, but there is a minimum point, there is a high density of states, there is a mutual attraction between magnetorotons, and, apparently, there are long lifetimes of such spin magnetorotons. The latter appear due to the significant slowing down of the relaxation processes, the difficulty of simultaneously fulfilling the laws of energy, momentum, and spin conservation during the decay from the roton minimum. This circumstance made it possible to create in GaAs quantum wells at PM $\nu = 2$ phase the macroscopic ensembles of CSFMs with a high degree of spatial coherence. Furthermore, in the MgZnO/ZnO heterostructures, considered here in the FM phase, a hint of macro-filled states has also been obtained as a nonlinear anomalous growth of the anti-Stokes component SE well beyond the thermodynamically equilibrium

distribution [34]. This line of research is up and coming, and further interest is in the study of such macro-filled states, the achievement for their spatial coherence, and the formation of SE condensates.

The depth of the roton minimum in the dispersion of the lowest spin excitations is directly related to the thermodynamic properties of the ferromagnet itself. It is known that FM state $\nu = 2$ is destroyed at significantly lower temperatures [3] than the QH ferromagnet $\nu = 1$, where the critical temperature is equal to the Zeeman energy [35]. Moreover, it is known that the destruction of a FM order occurs through the formation of domains of the opposite phase, and the critical temperature of such a process increases with the concentration of electrons. In this paper, we did not analyze the thermodynamic properties. However, it should be noted that, since the mechanism of nucleation of the opposite phase is attributed to the presence of a magnetoroton minimum in the SE dispersion, the temperature destruction of the spin order should also be associated with the energy of the lowest excitation, composed of magnetorotons. This energy increases with the density of electrons, and at the same time it is quite below the Zeeman energy.

Besides the negative sign and magnetoroton peculiarities, the measured momentum dispersion of the lowest energy SEs at $\nu = 2$FM carries information of the scale of the many-particle energy for electrons on LLs. One may conclude this by close values of the many-particle energies in Fig. 2 with analogous energy contributions to SEs at $\nu = 1$. These data once again indicate the strong renormalization of the exchange and correlation energies for QH states with $r_s \gg 1$ from the scale $e^2/\varepsilon \ell_B$ to $\hbar \omega_c$, which grows linearly with electron density at a fixed filling factor [13,14]. These issues concern not just the energies of collective excitations but also the renormalized mass of Fermi-liquid quasiparticles in these systems, their Landau quantization, previously probed by magneto-PL [31], also the renormalized spin-splittings of LLs extracted from the sequence of Ising ferromagnets at different integer filling factors. All these facts witness that many-particle energy scale for 2D electrons at $r_s \gg 1$ reduces and gets proportional to the electron density instead of its square root. Or, alternatively, the energy spectrum more resembles the quantized levels for weakly interacting Fermi-liquid quasiparticles.

VIII. CONCLUSION

In conclusion, we discovered an anomalous behavior of SEs in the quantum Hall ferromagnet at $\nu = 2$ with a strong Coulomb interaction and the Wigner-Seitz parameter r_s from 5.5 to 9. To that end, Raman scattering experiments were performed on MgZnO/ZnO high-quality heterostructures, containing 2DES with different densities. Hence, the momentum-dispersions of SEs were explicitly measured. It was found that the SE has a conspicuous negative dispersion in the long-wavelength limit. The steepness of the dispersion increases with electron density. This behavior was explained as a repulsion of the two lowest spin-flip modes. The dispersions have been analyzed by both numerical simulations in the frameworks of exact diagonalization of the

energy spectrum for a finite number of electrons and within the statically screened HFA. The calculations agree well with the experimental data and reveal the formation of the magnetoroton minimum at $ql_B \sim 1$. In addition, the calculations show the energy gain for two or more clumped SEs from the magnetoroton minima. This is a prerequisite for the phase transition back to the PM phase. Last but not least, we experimentally observed an anomalous enhancement of the anti-Stokes Raman component of SEs, which is evidence of their macroscopic accumulation in the sys-tem. This is promising, since these excitations carry integer spin.

[1] J. Falson, Y. Kozuka, J. H. Smet, T. Arima, A. Tsukazaki, and M. Kawasaki, Appl. Phys. Lett. **107**, 082102 (2015).

[2] J. Falson, D. Maryenko, B. Friess, D. Zhang, Y. Kozuka, A. Tsukazaki, J. H. Smet, and M. Kawasaki, Nat. Phys. **11**, 347 (2015).

[3] A. B. Van'kov, B. D. Kaysin, and I. V. Kukushkin, Phys. Rev. B **96**, 235401 (2017).

[4] J. Falson, I. Sodemann, B. Skinner, D. Tabrea, Y. Kozuka, A. Tsukazaki, M. Kawasaki, K. von Klitzing, and J. H. Smet, arXiv:2103.16586.

[5] C. Kallin and B. I. Halperin, Phys. Rev. B **30**, 5655 (1984).

[6] P. Plochocka, J. Schneider, D. Maude, M. Potemski, V. Umansky, I. Bar-Jospeh, J. Groshaus, Y. Gallais, and A. Pinczuk, *Journal of Physics Conference Series, 11th International Conference on Optics of Excitons in Confined Systems* (Institute of Physics Publishing, Bristol, 2010).

[7] V. E. Bisti, A. B. Van'kov, A. S. Zhuravlev, and L. V. Kulik, Phys. Usp. **58**, 315 (2015).

[8] L. V. Kulik, A. V. Gorbunov, A. S. Zhuravlev, V. B. Timofeev, S. Dickmann, and I. V. Kukushkin, Sci. Rep. **5**, 10354 (2015).

[9] S. M. Girvin, A. H. MacDonald, and P. M. Platzman, Phys. Rev. Lett. **54**, 581 (1985).

[10] S. F. Liou, F. D. M. Haldane, K. Yang, and E. H. Rezayi, Phys. Rev. Lett. **123**, 146801 (2019).

[11] L. V. Kulik, A. S. Zhuravlev, S. Dickmann, A. V. Gorbunov, V. B. Timofeev, I. V. Kukushkin, and S. Schmult, Nat. Commun. **7**, 13499 (2016).

[12] L. V. Kulik, A. S. Zhuravlev, L. I. Musina, E. I. Belozerov, A. B. Vankov, O. V. Volkov, A. A. Zagitova, I. V. Kukushkin, and V. Y. Umansky, (to appear in Nature Communications in 2021).

[13] A. B. Van'kov, B. D. Kaysin, S. Volosheniuk, and I. V. Kukushkin, Phys. Rev. B **100**, 041407(R) (2019).

[14] A. B. Van'kov and I. V. Kukushkin, Phys. Rev. B **102**, 235424 (2020).

[15] Y. Kozuka, A. Tsukazaki, D. Maryenko, J. Falson, C. Bell, M. Kim, Y. Hikita, H. Y. Hwang, and M. Kawasaki, Phys. Rev. B **85**, 075302 (2012).

[16] A. B. Vankov, B. D. Kaysin, and I. V. Kukushkin, Phys. Rev. B **98**, 121412(R) (2018).

[17] M. A. Eriksson, A. Pinczuk, B. S. Dennis, S. H. Simon, L. N. Pfeiffer, and K. W. West, Phys. Rev. Lett. **82**, 2163 (1999).

[18] L. V. Kulik, I. V. Kukushkin, S. Dickmann, V. E. Kirpichev, A. B. Vankov, A. L. Parakhonsky, J. H. Smet, K. von Klitzing, and W. Wegscheider, Phys. Rev. B **72**, 073304 (2005).

[19] S. M. Dickmann and B. D. Kaysin, Phys. Rev. B **101**, 235317 (2020).

[20] F. D. M. Haldane, Phys. Rev. Lett. **55**, 2095 (1985).

[21] W. Luo and T. Chakraborty, Phys. Rev. B **93**, 161103(R) (2016).

[22] V. E. Kozlov, A. B. Van'kov, S. I. Gubarev, I. V. Kukushkin, V. V. Solovyev, J. Falson, D. Maryenko, Y. Kozuka, A. Tsukazaki, M. Kawasaki, and J. H. Smet, Phys. Rev. B **91**, 085304 (2015).

[23] A. V. Schepetilnikov and Yu. A. Nefedov (to be published).

[24] M. Dobers, K. von Klitzing, and G. Weimann, Phys. Rev. B **38**, 5453 (1988).

[25] S. Koch, R. J. Haug, K. von Klitzing, and M. Razeghi, Phys. Rev. B **47**, 4048 (1993).

[26] E. P. De Poortere, E. Tutuc, S. J. Papadakis, and M. Shayegan, Science **290**, 1546 (2000).

[27] J. Jaroszynski, T. Andrearczyk, G. Karczewski, J. Wrobel, T. Wojtowicz, E. Papis, E. Kaminska, A. Piotrowska, Dragana Popovic, and T. Dietl, Phys. Rev. Lett. **89**, 266802 (2002).

[28] J. C. Chokomakoua, N. Goel, S. J. Chung, M. B. Santos, J. L. Hicks, M. B. Johnson, and S. Q. Murphy, Phys. Rev. B **69**, 235315 (2004).

[29] D. Maryenko, J. Falson, Y. Kozuka, A. Tsukazaki, and M. Kawasaki, Phys. Rev. B **90**, 245303 (2014).

[30] A. P. Smith, A. H. MacDonald, and G. Gumbs, Phys. Rev. B **45**, 8829 (1992).

[31] V. V. Solovyev and I. V. Kukushkin, Phys. Rev. B **96**, 115131 (2017).

[32] I. V. Kukushkin and S. Schmult, Phys. Rev. B **101**, 235152 (2020).

[33] A. B. Van'kov, B. D. Kaysin, and I. V. Kukushkin, JETP Lett. **107**, 110 (2018).

[34] B. D. Kaysin, A. B. Van'kov, and I. V. Kukushkin, JETP Lett. **112**, 62 (2020).

[35] A. S. Zhuravlev, A. B. Vankov, L. V. Kulik, I. V. Kukushkin, V. E. Kirpichev, J. H. Smet, K. v. Klitzing, V. Umansky, and W. Wegscheider, Phys. Rev. B **77**, 155404 (2008).